



Experimental and Numerical Research of the Flow Features Around the Building Pairs with Different Types

Deniz GÖLBAŞI¹, Ertan BUYRUK², Koray KARABULUT^{1*}

¹Sivas Cumhuriyet University, Sivas Vocational High School, Department of Electric and Energy, Sivas, TURKEY

²Sivas Cumhuriyet University, Engineering Faculty, Department of Mechanical Engineering, Sivas, TURKEY

Received: 11.02.2018; Accepted: 28.11.2018

<http://dx.doi.org/10.17776/csj.393304>

Abstract. Flow structure on the building is a primary factor in dispersing of air pollutants into and around of the building. Therefore, it is required to determine air motions outside of the building. In this study, flow features at the vicinity of the two building models with rooftop and without rooftop having same dimensions were investigated experimentally and numerically. In the experimental part of the study, flow structures around buildings having dimensions of 5x5x5cm without rooftop and 5x5x5cm with 30° slope and rooftop were examined firstly by placing one by one and afterwards they were analysed by leaving a distance of 13.75cm as binary placed (with rooftop, without rooftop and with and without rooftop) by using Particle Image Velocimetry (PIV). In the numerical part of the study, experimental works carried out by placing binary building was researched by using ANSYS Fluent 12.1 software with k-ε turbulence model as three dimensional, steady and the obtained numerical results were compared with experimental results. Instantaneous velocity fields were firstly obtained at the experiments and then stream lines $\langle \Psi \rangle$ and vortex peer curves $\langle \omega \rangle$ were plotted by using these datas. Average equivalent velocity curves distributions in the x and y directions were also investigated both for building models. The results showed that the vortexes occurred behind the building for the building without rooftop (model A) were symmetric with each other whereas they were not symmetric at the building with rooftop (model B). Also, the lengths of the vortexes at the rear of the model B increased 7.5% according to model A. The obtained result demonstrated that the rooftop had an effect on the flow structure. However, it was seen that the results were confirmed with a deviation of 3% when compared experimental results with numerical.

Keywords: Building aerodynamic, Particle Image Velocimetry (PIV), Flow separation.

Farklı Tiplerdeki Bina Çiftleri Etrafındaki Akış Özelliklerinin Deneysel ve Sayısal Olarak Araştırılması

Özet. Bina üzerindeki akış yapısı, bina içine ve etrafına hava kirleticilerinin yayılmasında birinci derecede etkindir. Bu nedenle, bina dışındaki hava hareketlerinin belirlenmesi gerekmektedir. Bu çalışmada, aynı boyutlara sahip çatılı ve çatısız iki bina modeli etrafındaki akış özellikleri deneysel ve sayısal olarak incelenmiştir. Çalışmanın deneysel kısmında, 5x5x5cm boyutlarında çatısı olmayan ve 5x5x5cm boyutlarında 30° eğime sahip çatılı bina modelleri etrafındaki akış yapıları öncelikle binalar tek tek yerleştirilerek ve sonrasında ise binalar aralarında 13.75cm mesafe bırakılıp (çatısız, çatılı ve çatılı-çatısız) ikili olarak yerleştirilerek Parçacık Görüntülemeli Hız Ölçüm Tekniğinin (PIV) kullanılmasıyla incelenmiştir. Çalışmanın sayısal kısmında ise iki bina yerleştirilerek yapılan (çatılı ve çatısız) deneysel çalışmalar k-ε türbülans modeli ANSYS Fluent 12.1 bilgisayar programı kullanılarak üç boyutlu, zamandan bağımsız olarak incelenmiş ve elde edilen sayısal sonuçlar deneysel sonuçlarla karşılaştırılmıştır. Deneyler neticesinde, öncelikle anlık hız alanları elde edilmiş ve sonra bu veriler kullanılarak akım çizgileri $\langle \Psi \rangle$ ve girdap eş düzey eğrileri $\langle \omega \rangle$ çizilmiştir.

Ayrıca, her iki bina modeli için x ve y yönündeki ortalama eşdeğer hız eğrileri dağılımları incelenmiştir. Sonuçlar, çatısız bina (model A) için bina arkasında oluşan girdaplar simetrik iken çatılı binada (model B) simetrik olmadığını göstermiştir. Ayrıca, model B'nin arkasındaki girdapların uzunlukları model A'ya göre % 7.5 artmıştır. Elde edilen sonuç, çatının akış yapısı üzerinde bir etkisinin olduğunu kanıtlamıştır. Bununla birlikte, deneysel ile sayısal sonuçlar karşılaştırıldığında % 3' lük bir sapma ile doğrulandığı görülmüştür.

Anahtar Kelimeler: Bina aerodinamiği, Parçacık Görüntülemeli Hız Ölçümü (PIV), Akış ayrılması.

1. INTRODUCTION

The separation zones resulting from the wind interaction between the building and its immediate surroundings are of great importance for determining the wind forces acting on the buildings, multiple vortex systems interacting with the building and for considering the appropriate design parameters. The flow structure on the building is the first degree factor in dispersing of air pollutants into and around of the building. In order to find of these effects, air movements outside the building should be determined. The flow vortex movements seen in front of the building cause by raising particles such as dust, soil, leaves, rain and snow found in ground level [1]. For these reasons, the knowledge of the flow structure and physic on the building contributes in terms of solving both design and technical problems. The influencing each other of two objects which is found in flow domain is discussed in the cases of enough close to each other of two objects or rearward object is in the track area of the front object [2]. The distance between the buildings makes the flow much more complicated in the stream around the buildings placed side by side. Especially, it has a direct influence on the formation and development of the trace area formed behind the buildings and jet flow between the buildings. When stubby objects are coexisted in flow domain, flow structures around these objects interact with each other. Tutar and Oguz [3] placed square model buildings in singular and binary form and calculated the turbulent flow field around the building models for different wind angles and geometric arrangements by using the finite volume method. They compared results found by using RNG sub-grid scale method with results of experimental wind tunnel. As a result, it was seen that there was a compatibility between numerical and experimental results on especially building

roof for single building configuration. In an another study, Blocken and Carmeliet [4] researched effects of WDR (wind-driven rain is rain which is given a horizontal velocity component by the wind) on the building models by carrying out experiments of PIV (particle image velocimetry) and wind tunnel and compared these obtained results with Fluent software program (CFD). They studied a low building model, a high building and the mutual influence of these two buildings. They found that the presence of low buildings was not a shield for the multi-storey building by the WDR and the wind and increased the strength of the WDR on the higher building front by increasing the fixed vortex force. Gölbasi et al. [5] investigated numerically and experimentally the flow structures around the four different building models composed of square without roof, short, long and broad with roof. They found that the vortex sizes behind the building changed due to the geometry of the building and the largest vortex formed in a large building model. In an another study, Gölbasi et al. [6] examined the flow characteristics of vicinity of two building models having different heights for two different measurement surfaces ($y/h=0.5$ ve $y/h=1$) as top view and for $y/h=0.5$ as side view by using Particle Image Velocimetry (PIV). The study was also solved numerically by using ANSYS 12.0 Fluent (finite volume method) with k- ϵ turbulence model as three dimensional, steady. They determined that as a result of separating of the coming wind from edges and corners of buildings, reverse flow zones occurred in the front, rear, along the side walls of the buildings and on the roof surfaces. And also, turbulence intensities in the blending layer separating inverse and free flow zones increased. Pollution distribution around a group of buildings in Montreal's city center was examined for two different turbulence models with wind tunnel experiments by Blocken and Stathopoulos [7]. The

results of wind tunnel was verified by CFD results with high-definition. The Reynolds Mean Navier-Stokes (RANS) and Large Eddy Simulation (LES) models were used as the turbulence models and it was seen that the LES approach was consistent with CFD and experimental results for both wind directions. Wind tunnel experiments were conducted in order to investigate the mutual interaction effects between twin super long buildings with aerodynamic regulation by Yan and Li [8]. Contour drawing of the mutual interaction effects were presented for evaluating wind induced reaction, local surface pressure coefficients and mutual interaction effects on global aerodynamic loads, quantitatively in the study. The results showed that the dynamic wind loads and responses significantly increased in the crucial sequential and distorted arrangements of the twin towers and that negative pressure coefficients of the lowest peak were larger than the non-interactive ones by about 30%.

Knowing of the flow structures on the buildings contributes both in terms of design and preventing to mix particles such as dust, soil, leaves, rain and snow found in ground level to building inner environment by raising with vortex motions. Therefore, in this study, flow structures around buildings having dimensions of 5x5x5cm without rooftop and 5x5x5cm with 30° slope and rooftop were examined experimentally firstly by placing one by one and afterwards they were analysed by leaving a distance of 13.75cm as binary placed (with rooftop, without rooftop and with and without rooftop) by using Particle Image Velocimetry (PIV). Also, the experimental work carried out by placing binary building was numerically researched by using ANSYS Fluent 12.1 software program with k- ϵ turbulence model as three dimensional, steady and the obtained numerical results were compared with experimental results. Instantaneous velocity fields were firstly obtained at the experiments and then stream lines $\langle \Psi \rangle$ and vortex peer curves $\langle \omega \rangle$ were plotted by using these datas. However, average equivalent velocity curves distributions in the x and y directions were also investigated both for building models.

2. MATERIAL AND METHOD

Experiments in this study were carried out by using Particle Image Velocimetry (PIV) in water channel working as closed circuit with open surface found in the Fluid Dynamics Laboratory of Mechanical Engineering Department in the Cukurova University. Water channel composes of two water reservoirs produced from fibreglas material and transparent acrylic part assembled between these reservoirs called as experiment channel which has 750mm height, 1000mm wide and 9000mm length. Motion of the water between two water reservoirs is driven by a 15 kW centrifugal pump. The rotation speed of the pump is shifted by a velocity control unit with frequency controller unit to carry out experiments in different velocities. Centrifugal pump pumps the water to tank at the inlet by sucking from the water tank at the outlet. During the tests, a flow-regulating comb system was installed outlet of the inlet tank to ensure uniform of the flow along the experiment channel and however, the connection was provided by narrowing by a ratio of 2:1 between the outlet of the inlet reservoir part and the test channel joint. To minimize the thermal interaction of water channel and particle circulation systems, the laboratory was kept at a nominal room temperature of 22°C. Laboratory glasses were also covered with special blinds to protect the laser beam from sunlight. The view of the test channel is shown in Fig. 1.



Figure 1. Test channel.

In general, velocity measurement with the PIV technique consists of two steps as visualization and image processing. Small particles following the flow are added to the flow field. These particles are illuminated sequential two times in a short time interval by a light source on the surface to be

measured. The time difference, Δt , between the sequential illuminations of light source (mostly laser) is adjusted depending on average flow rate and the magnification of the image. During the time between the two lights, the particles move with the local flow velocity. The light emitted by the particles is perceived by a high-resolution camera placed perpendicular to the light layer and recorded on two frames. The obtained photographic PIV records are then digitized and transferred to the computer using a scanner [9].

Working principle of PIV are shown in Fig. 2. Two building models made of transparent acrylic material were used to examine the flow structure. During the tests, the water height was fixed at 0.45m. The front point of plane platform was thinned by chamfering so as not to disturb the flow. In order to avoid turbulence effects, the cylinder model was mounted 1.5m distance from the inlet on the plane platform from the flow direction. Experiments were carried out for the case of the free flow rate with 210mm/s. The schematic view of the test area in the water channel was given in Figure 3.

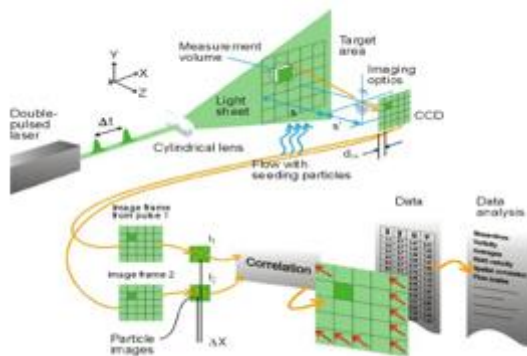


Figure 2. PIV working principle [10].

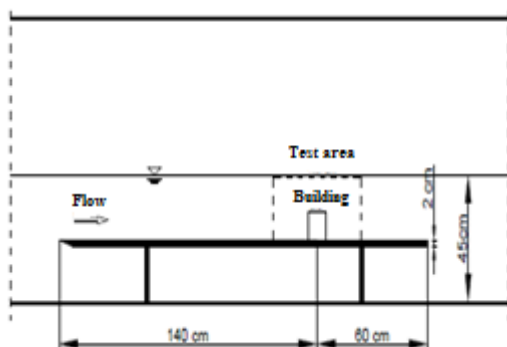


Figure 3. Schematic view of the plane platform.

3. TOP VIEW MEASUREMENT SURFACES

In Fig. 4, when the camera was placed on the top of the channel, laser was located in front of the building for a top view and an experimental setup was formed by placing a mirror with a 45° slope in front of the camera. The symmetry surface shown in Fig. 5 was taken at $z/H = 2$ for top view.

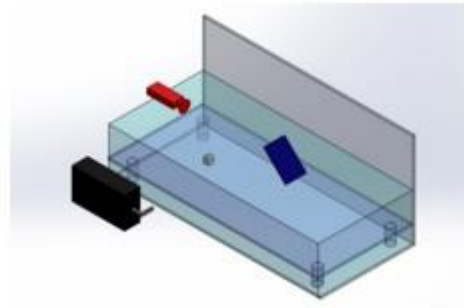


Figure 4. Top view measurements.

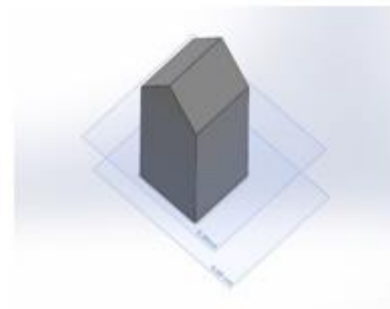


Figure 5. Top view measurement surface.

4. FLOW BETWEEN SINGLE BUILDING MODELS

Shapes with three appearances are pointed out in Figs. 6 and 7 for used square building models without rooftop at dimensions of $5 \times 5 \times 5$ cm and with rooftop at dimensions of $5 \times 5 \times 5$ cm with 30° inclined, in this study.

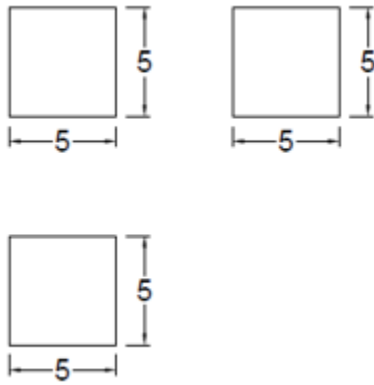


Figure 6. Square model (A) without rooftop.

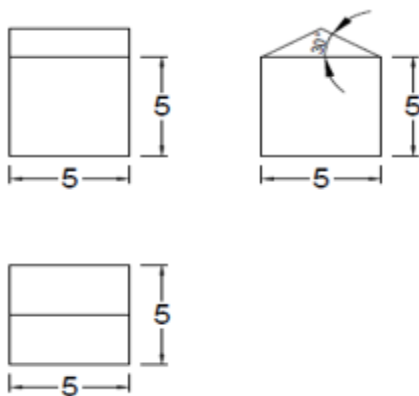


Figure 7. Square model (B) inclined and rooftop.

5. EXPERIMENTAL RESULTS

5.1. Experimental Results of Single Building

In the result of the experiments, the flow structure formed around building was presented as stream lines $\langle \psi \rangle$ and vortex peer curves (ω). While the velocity vectors show the direction and distribution of the flow in the obtained datas, the flow lines facilitate the understanding of the instantaneous flow datas. Peer curves formed by the effect of turbulent boundary layer. Curvilinear curves (peer) are given by coloring. In this coloring, blue and red colors more clearly express the centers of vortices. When positive (blue) show that the vortices follow the motion in the opposite clockwise, negative (red) indicates the clockwise.

The flow structure around the square building model without rooftop at dimensions of 5x5x5cm is exhibited in Fig. 8. From the stop point (Sab) formed in the front region of the model, the flow

was divided into two parts, upward and downward (Fig. 8a). The upflow formed a vortex region (F1) by separating from left side corner of the model. A stop point (saddle point-S1) occurred in the right part of this vortex. When the side left separation point of the model reached to N1 point, its length and thickness were $XR=29.1\text{mm}$ and 10.1mm , respectively. The reason of the separation from the surface was that the kinetic energy at the separation point was less intensity according to pressure energy. The downflow formed a vortex region by leaving the side right corner of the model. A stop point (saddle point-S2) occurred in right part of this vortex. When side right separation point of the model reached to N2 point, its length and thickness were measured as $XR=25.97\text{mm}$ and 9.8mm , respectively. Shear layers from the top and bottom surfaces interacted at rear region of the model and formed overlapped symmetric vortex pair. A vortex positioned at the top and turning in the clockwise formed. This is also the region where negative vortex forms and the peer-vortex curves are shown as red line (Fig. 8b). F4 vortex positioned at the bottom side turns the opposite clockwise and this region where the positive vortex occurred. F3 and F4 vortex regions formed in the results of energy losses and separation of the boundary layer according to separation points at the top and bottom parts of the model. The size of the separation region at the rear surfaces such as the building and vehicle affected direct resistance force [11]. It was determined that the length of the separation region at the rear of the model was 50mm. The stop point occurred in the middle region due to equal vortex sizes of the F3 and F4 at the rear of the building.

Fig. 9 shows the flow structure around the building (Model B) with 30° inclined and rooftop at dimensions of 5x5x5cm. In generally, flow structure of model B is similar to that of the model A (without rooftop) but some differences attracts attention. The symmetrical structure was distorted at the vortices which were formed rear of the model and positioned one after the other due to the rooftop. It is considered that the reason of this is the model with rooftop and close to roof of the building in terms of surface taken in the image. Vortex at the

bottom is relatively small. The separation region separated to upward flow extends to N1 point and its length and thickness were determined as $X_R=26.28\text{mm}$ and 10.1mm , respectively (Fig. 9a). However, the separation region separated to downward flow extends to N2 point and the length and thickness were measured as $X_R=40,36\text{mm}$ and 12.7mm . In this surface, the length and thickness of separation region also increase, which points out increasing of the boundary layer thickness. Vortex positioned at the top part and turning the clockwise from the vortex pairs at the rear of the building has a larger area and the coordinates of F3 vortex central are of the point at $x=104.04\text{mm}$ and $z=139.37\text{mm}$. This is region that vortex turns the clockwise and peer vortex curves are shown as red color (Fig. 9b). Stop point (S3) occurred at the below by leaving the rear of the building and it formed at the points of $x=144.44\text{mm}$ and $z=119.05\text{mm}$. When F3 positioned at top and rear of the building expanded, vortex became small at the bottom. Boundary layer development and requirement to development distance of vortex regions can be shown as reason of observed variations at sizes of the vortex regions formed rear of the building due to rooftop by moving away from the walls of the model.

Average equivalent u velocity curves distributions around the model A placed as single in the x direction are shown in Figs. 10a and b for symmetry surfaces of $z/H=0.5$ and $z/H=1$, respectively. A separated flow region consisted at the back of the building as illustrated in Fig. 10a.

The formed this separated flow region extends to $x/H=0.71$ point. Separated flow area was not obtained for $z/H=0.1$ symmetry surface at the back region of the building and the flow moved from the building roof without leaving the surface (Fig. 10b). Therefore, the vortex didn't compose at the side and back regions of the building and velocity values of u around the building increased.

In the y direction, distributions of average equivalent v velocity curves for model A are pointed out in Figs. 11a and b at the symmetry surfaces of $z/H=0.5$ and $z/H=1$, respectively. When v velocity component curves in the vertical direction are examined, straight and dashed lines show upward and downward flow area, respectively. The curves of v velocity indicate a symmetric view in Fig. 11a. Upward flow area possesses at front section of the building in especially top-side section. Downward flow that has higher energy dominates at the bottom-side section of the building. When there is the upward flow area at the bottom section of the building, downward flow region exists at the top-back section of the building. In Fig. 11b, an image was taken similar to profile of v velocity on the symmetry surface of $z/H=0.5$ at the front section of the building and a profile that slipping forward at the top rear of the building was formed. The upward flow region occurred on the building side surface by exactly forming a different image at the back-bottom side of the building.

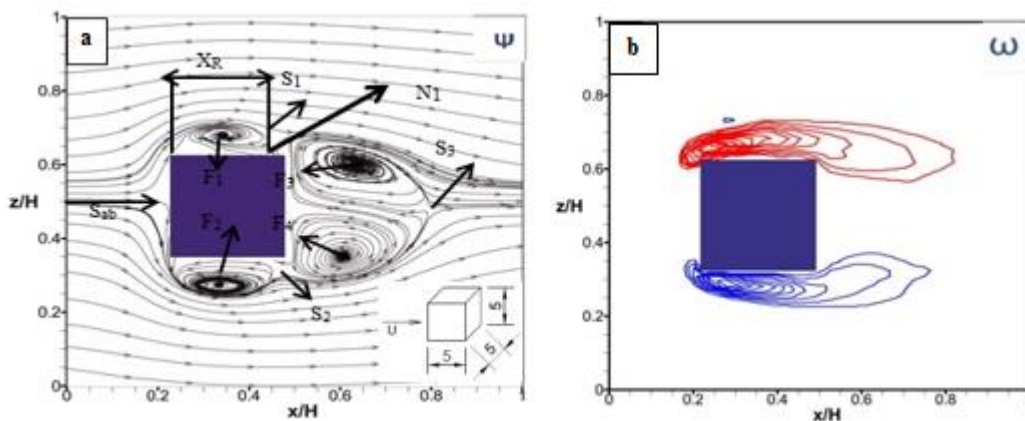


Figure 8. Top view for flow around building (model A) without rooftop at $z/H=0.5$ surface **a)** Stream line $\langle\psi\rangle$ **b)** $\langle\omega\rangle$, increment values of min. and vortex curves are $\langle\omega_{\min}\rangle=\pm 4\text{s}^{-1}$ and $\Delta\langle\omega\rangle=2\text{s}^{-1}$

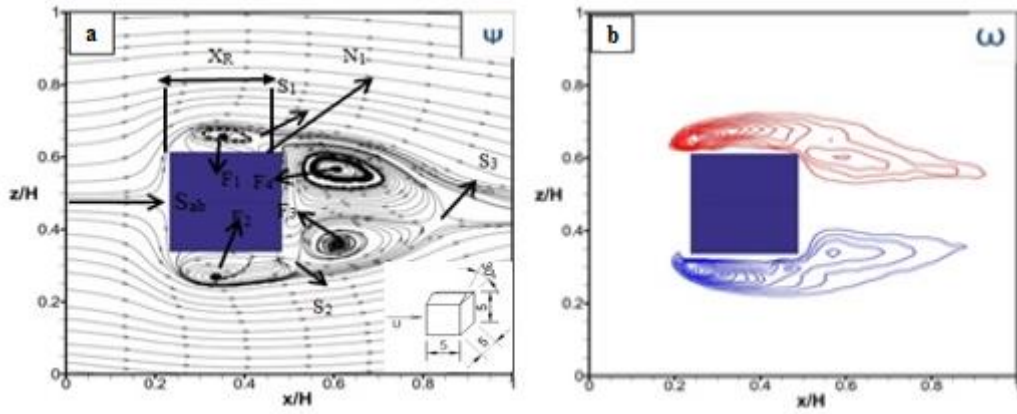


Figure 9. Top view for flow around building (model B) with rooftop at $z/H=0.5$ surface **a)** Stream lines $\langle \psi \rangle$ **b)** vortex curves $\langle \omega \rangle$, increment values of min. and vortex curves are $\langle \omega_{min} \rangle = \pm 4s^{-1}$ and $\Delta \langle \omega \rangle = 2s^{-1}$

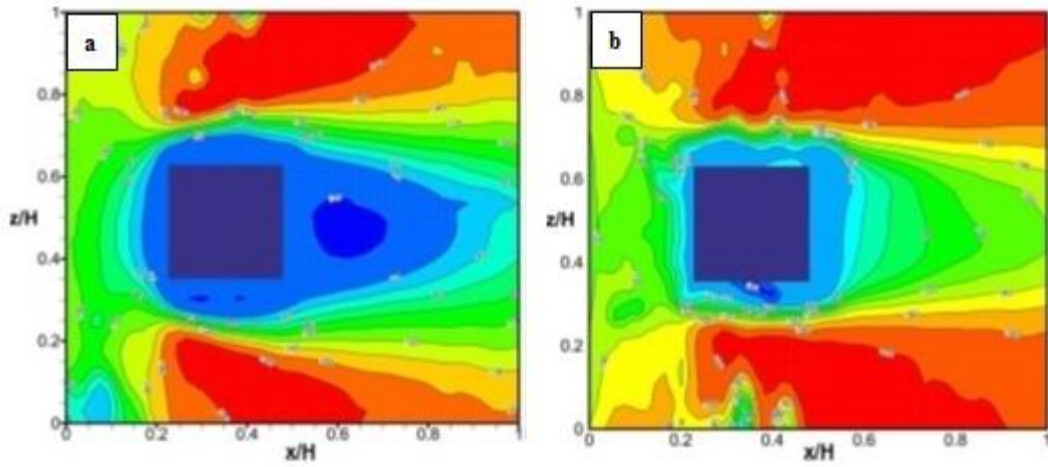


Figure 10. Average equivalent u velocity curves distributions for flow around building (model A) placed as single in the x direction at surfaces of **a)** $z/H=0.5$ **b)** $z/H=1$

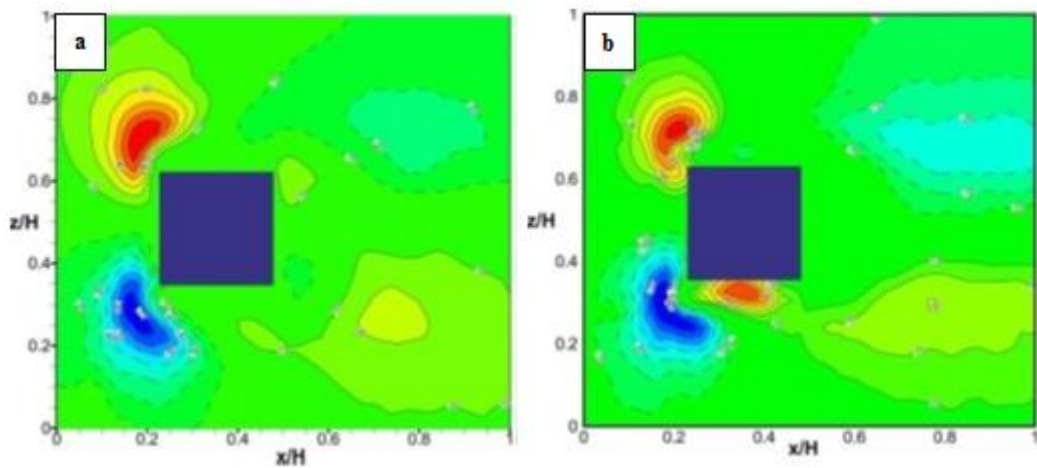


Figure 11. Average equivalent v velocity curves distributions for flow around building (model A) placed as single in the y direction at surfaces of **a)** $z/H=0.5$ **b)** $z/H=1$

Distributions of average equivalent u velocity curves are shown in Figs. 12a and b for x direction of the flow around the model B with the single building at the symmetry surfaces of $z/H=0.5$ and 1, respectively. A separated flow region was come into existence as seen in Fig. 12a. This occurred separated flow region extends to point of $x/H=0.75$. Any separated flow was not obtained for symmetry surface of $z/H=1$ at the side surfaces of the building and the flow conducted from the building roof without leaving the surface (Fig. 12b). However, the separated flow region composed at the back area of the building.

In Figs. 13 a and b, average equivalent v velocity curves distributions for y direction of the flow around the model B are illustrated at the symmetry

surfaces of $z/H=0.5$ and 1, respectively. The curves of the y velocity component show a symmetric view in Fig. 13a. Upward flow region dominates especially building top side section at the front of the building. When there was downward flow area at the top back section of the building, upward flow region existed at the bottom section. The velocity profiles of v existing back of the building advance by reaching backward. In Figure 13b, a similar view was taken in v velocity profile at the symmetry surface of $z/H=0.5$ for the building front section. A forward developing profile occurred at the back, top and bottom region of the building. Upward flow area comprised at the building side surface for the back bottom region of the building.

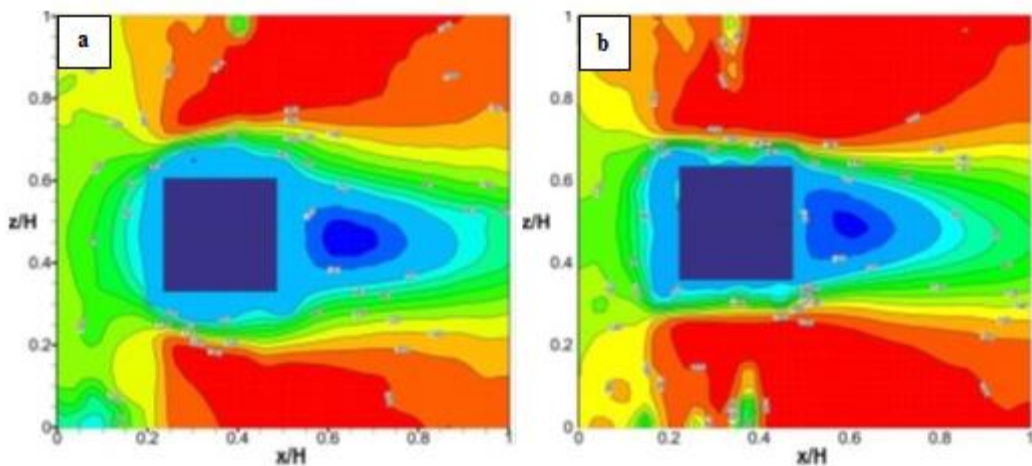


Figure 12. Average equivalent u velocity curves distributions for flow around building (model B) placed as single in the x direction at surfaces of a) $z/H=0.5$ b) $z/H=1$

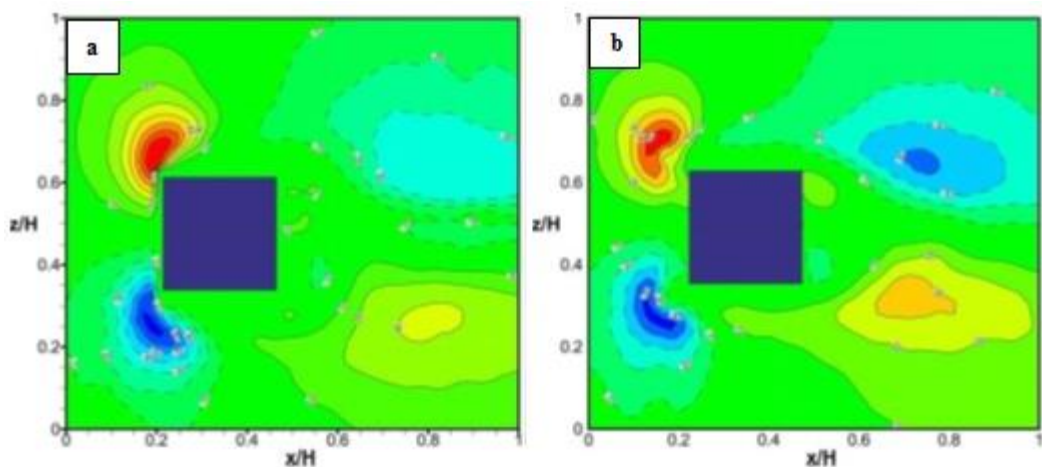


Figure 13. Average equivalent v velocity curves distributions for flow around building (model B) placed as single in the y direction at surfaces of a) $z/H=0.5$ b) $z/H=1$

5.2. Experimental Results of Binary Buildings

In Fig. 14, the flow structures of two building models without rooftop (model A) at dimensions of 5x5x5cm by placing on plate in the channel were investigated.

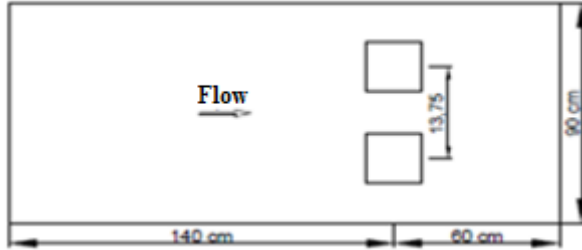


Figure 14. Schematic view of two building models.

As can be seen in Fig. 8, the flow structures resemble with streamlines and vortex curves at single building model without rooftop. Due to the fact that two building models are the same, vortex sizes of the two models at the rear regions are about same (Fig. 15a). When vortices for two buildings at the side walls were examined, as vortex formed at both sides of the top building, it was observed that vortex was not formed at one region of the bottom building. The separation region at the upward flow extends to N1 point and the length and thickness are measured as $XR=30,36\text{mm}$ and $11,11\text{mm}$, respectively. However, the separation region at the downward flow extends to N2 point and length and thickness are $XR=28,34\text{mm}$ and $12,3\text{mm}$, respectively. When the vortices formed at the rear of the building were investigated, it was seen that they had symmetric structure according to each other. At the top part formed vortex F3 turns clockwise and it has central coordinates of $x=106,307\text{mm}$ and $z=210,186\text{mm}$. As also shown in Fig. 15b, vortex peer curves are indicated with red color. The coordinates of S1 point were determined as $x=136,267\text{mm}$ and $z=194,41\text{mm}$. When bottom building was researched, the flow separating from Sab2 point to upward was divided by separating from side-left corner of the model but it was not formed a distinct vortex structure. The right separation region at downward flow extends to N2 point and its length is $XR=32,2\text{mm}$ and its thickness is $12,1\text{mm}$. When the vortices formed at

the rear region of the bottom building were examined, it was seen that they were almost symmetrical structure each other. However, the length and thickness of the separation region at the rear of the model were determined as $38,5\text{mm}$ and $20,3\text{mm}$. The coordinates of the S2 point (stop point) are $x=134,243\text{mm}$ and $z=53,4137\text{mm}$.

The flow structures around the two building models whose dimensions are 5x5x5cm and with 30° inclined and rooftop are examined in Fig. 16. Because the two building models are the same, vortex sizes at the rear region of the two models are almost same (Fig. 16a). When the vortices were investigated in the side walls for two buildings, it was seen that formed vortices showed similarity each other. The separating region of the separating upward flow from Sab1 point on front wall of the top building model extends to N1 point and its length and thickness are determined as $XR=23,08\text{mm}$ and $8,81\text{mm}$, respectively. Separation region which is separated to downward flow extends to N2 point and the length and thickness are measured as $XR=21,4\text{mm}$ and $8,8\text{mm}$, respectively. When vortices were researched at the rear region of the building, it was seen that they were symmetrical structure each other. The coordinates of S1 point which is stop point are indicated as $x=144,365\text{mm}$ and $z=189,311\text{mm}$. When bottom building is investigated, the separation region of the separating upward flow from Sab2 point on front wall of the building extends to N3 point and the length and thickness of N3 are $XR=21,18\text{mm}$, $7,2\text{mm}$, respectively. The separation region of the separating downward flow extends to N4 point and the length and thickness are measured as $XR=33,5\text{mm}$, $9,1\text{mm}$, respectively. When the forming vortices at the rear region of the bottom building were investigated, it was seen that they had about a symmetrical structure. The forming vortex F7 at the top part turns the clockwise and its central coordinates are at the points of $x=101,449\text{mm}$ ve $z=61,29\text{mm}$. Here, the vortex peer curves are pointed out with red color (Fig.

16b). The coordinates of S2 are $x=146.389\text{mm}$ and $z=33.933\text{mm}$.

Average equivalent u and v velocity curves distributions for symmetry surface of $z/H=0.5$ around the binary models without rooftop (model A) at the x and y directions are shown in Fig. 17 a and b, respectively. Separated flow region occurred at the top-side and back areas of the building are seen in Fig. 17a. These occurred separated flow areas are equal magnitudes and extend to $x/H=0.55$ point. Velocity increments were obtained due to jet flow comprised between two buildings and the maximum velocity occurred in between two buildings. Symmetric equal velocity curves were formed in bottom and top sections (sharp corners)

of the flow direction at the building front (Fig. 17b). Upward flow regions at the building top sections and downward flow regions at the building bottom sections composed. There are small upward and downward flow regions at the sharp corners behind the building. Symmetric v equal velocity curves composed at the region close to side surfaces between the buildings. Upward flow regions close to top building and downward flow regions close to bottom building occurred. Symmetrical v flow curves composed at the sides close to channel walls on the building outside surfaces.

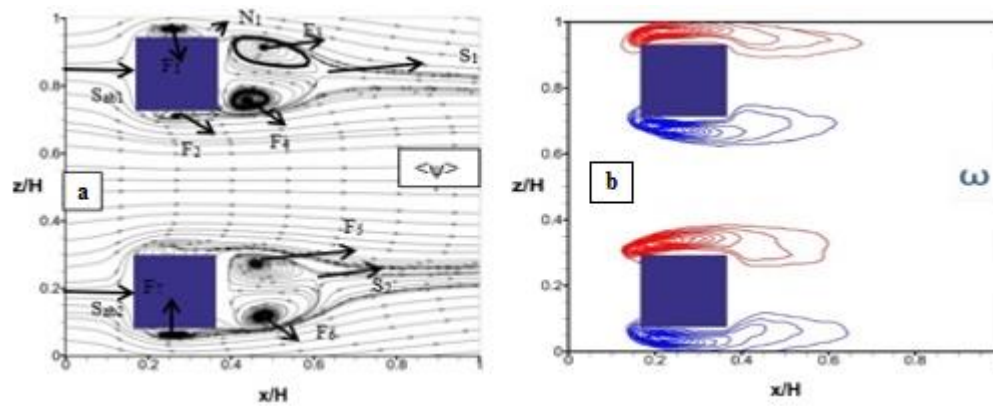


Figure 15. Flow around the model A for binary building at surface of $y/h=0.5$ time averaged **a)** Streamlines **b)** Vortex peer curves $\langle\omega\rangle$, increment values of min. and vortex peer curves are $\langle\omega_{\min}\rangle=\pm 4\text{s}^{-1}$ and $\Delta\langle\omega\rangle=2\text{s}^{-1}$

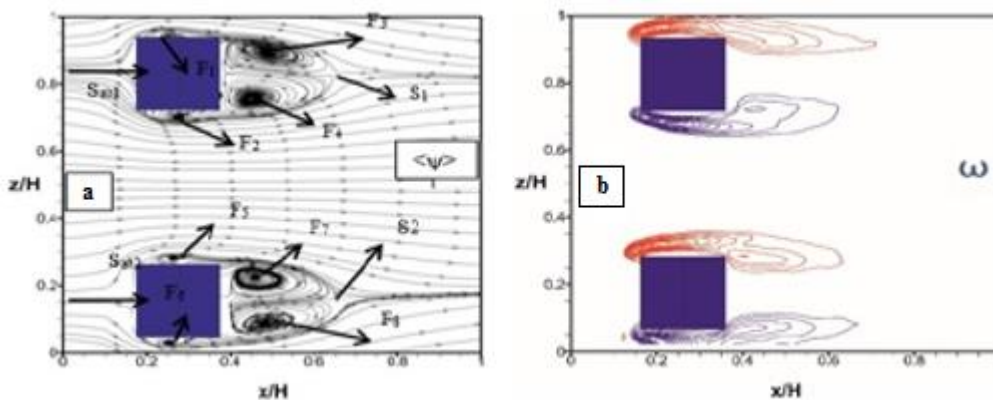


Figure 16. Flow around the model B for binary building at surface of $y/h=0.5$ time averaged **a)** Streamlines **b)** Vortex peer curves $\langle\omega\rangle$, increment values of min. and vortex peer curves are $\langle\omega_{\min}\rangle=\pm 4\text{s}^{-1}$ and $\Delta\langle\omega\rangle=2\text{s}^{-1}$

In Figs. 18 a and b, average equivalent u and v velocity curves distributions around the binary models of B with 30° inclined and rooftop are shown for the symmetry surface of $z/H=0.5$ at the x and y directions, respectively. Reverse flow regions occurred at the building back areas are seen in Fig. 18a. The occurred separated flow regions are equal magnitudes for two buildings and they extend to point of $x/H=0.62$. The separated flow region enlarges when compared to u equivalent velocity curves shown in Fig. 17a. The velocity augmentations are seen due to jet flow between buildings and they especially increase near the buildings. Maximum velocity was obtained between the two buildings. Non-uniform flows were seen at the front inlet sections of the buildings. The reason for this, it is considered that particles added to channel collapse on the tray and black tapes used in order to shut down the slots stick during the experiments. Equivalent velocity curves of u occurred around the buildings are compatible each other and symmetric. Symmetric v equivalent velocity curves composed in bottom and top sections (sharp corners) of the flow direction at the building front as seen in Fig. 18b similar to Fig. 17b. There are upward and downward flow regions at the top and bottom sections of the buildings. Small top and bottom flow regions occurred at the back of the building on the top and bottom sections of the sharp corners. There are symmetric v equivalent velocity curves at the area between the buildings near the side surfaces. As upward flow region was obtained at the near the top building, downward flow areas came into existence at the near the bottom building. Upward and downward flow areas relatively increased according to building model without rooftop. v flow curves that are symmetric to each other composed at the edges near the channel walls on the building outside surfaces. However, downward flow area occurred around the top building while upward flow region composed around the bottom building.

In Fig. 19, the flow structure around building models without rooftop (model A) and with rooftop and 30° inclined (model B) at dimensions of $5 \times 5 \times 5$ cm were investigated. When model B was positioned on top of the plate, model A was on the bottom part of the plate. Because the two building models are different, it is seen that the sizes of the vortices vary when the vortex sizes at the rear region of the two building models are examined (Fig. 19a). The lengths of the vortex at the rear of the model with rooftop (model B) increased 7.5% according to model without rooftop. For two buildings, when the vortices on the side walls are investigated, the sizes are almost same that of model without rooftop (model A). At the top building model, the separation region of the separating upward flow from the point of Sab1 on the building front wall extends to point of N1 and its length and thickness are $XR=23.88$ mm, 9.87 mm, respectively. However, the separation region of the separating downward flow is point of the N2 and the length and thickness are measured as $XR=17.82$ mm and 6.96 mm, respectively. When the forming vortices at the rear region of the building are evaluated, it is seen that they are symmetrical each other. F3 vortex that forms at the top part turns the clockwise and the coordinates of center are $x=105.094$ mm and $z=207.98$ mm. The vortex peer curves relating to this are displayed as red color in Fig. 19b. The coordinates of S1 point are $x=135.685$ mm and $z=183.311$ mm. While the bottom building is investigated, the separation region of the separating upward flow from the point of Sab2 on the building front wall extends to N3 and its length and thickness are $XR=21.45$ mm and 7.88 mm. Besides, the separation region of the separating downward flow extends to N4 point and its length and thickness are measured as $XR=32.39$ mm and 8.4 mm. The coordinates of stop point that is S2 are determined as $x=135.86$ mm and $z=34.39$ mm.

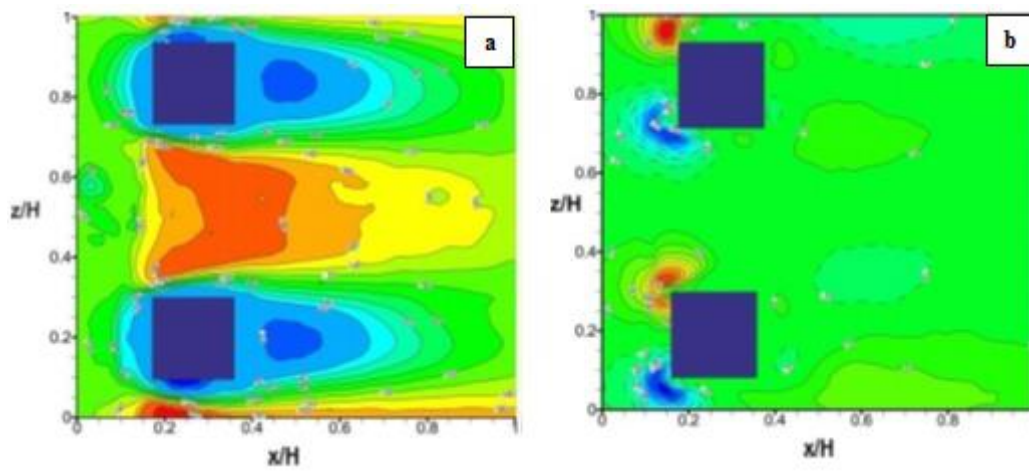


Figure 17. Average equivalent u and v velocity curves distributions for flow binary models without rooftop (model A) at the x and y directions at surfaces of $z/H=0.5$ a) u velocity b) v velocity

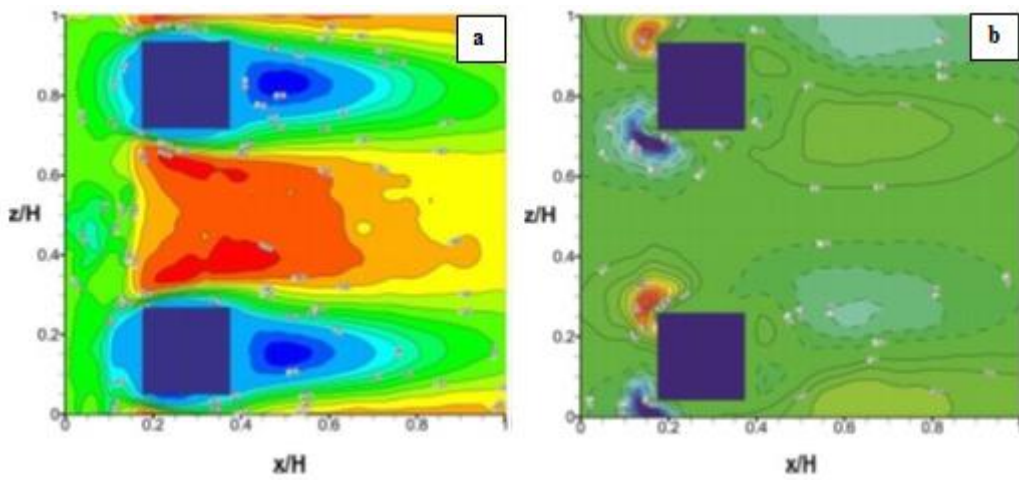


Figure 18. Average equivalent u and v velocity curves distributions for flow binary models without rooftop (model B) at the x and y directions at surfaces of $z/H=0.5$ a) u velocity b) v velocity.

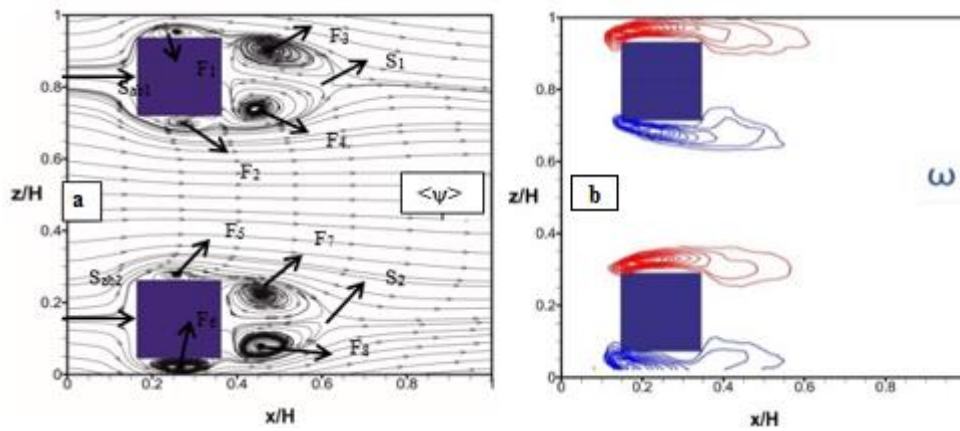


Figure 19. Flow around the models A and B for binary building at surface of $z/H=0.5$ time averaged a) Streamlines b) Vortex peer curves $\langle \omega \rangle$, increment values of min. and vortex peer curves are $\langle \omega_{min} \rangle = \pm 4s^{-1}$ and $\Delta \langle \omega \rangle = 2s^{-1}$

Average equivalent u and v velocity curves distributions around the binary models of model B with rooftop and 30° inclined and model A (without rooftop) for $z/H=0.5$ symmetry surface at the x and y directions are illustrated in Figs. 20 a and b, respectively. The separated flow area occurred back regions of the building are seen in Fig. 20a. The obtained these separated flow areas did not composed at equal magnitudes due to the different buildings models. As x/H extends to point of 0.52 for model A placed in the bottom, it reaches to 0.57 point for the model B positioned at the top. The velocity increments are seen between the two buildings because of the jet flow. Therefore, the maximum velocity occurred between the buildings.

Non-uniform flows were obtained at the front entrance. In Fig. 20b, the very different flow areas composed according to Figs. 17b and 18 b and v equivalent velocity curves were obtained at the bottom and top sections in front of the building. As upward flow section came into existence at the building top areas, downward flow section occurred at the bottom section of the building. V equivalent velocity curves that are non-symmetric to each other occurred at the region near the side surfaces between the building. When compared Fig. 18b with Fig. 20b, the 180° converted image according to one another was determined.

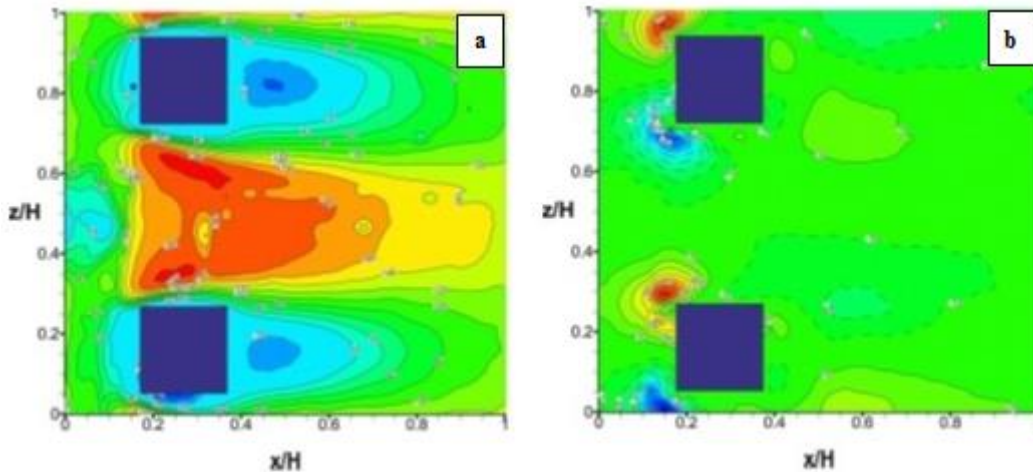


Figure 20. Average equivalent u and v velocity curves distributions for flow binary models of A and B at the x and y directions at surfaces of $z/H=0.5$ **a)** u velocity **b)** v velocity.

6. NUMERICAL RESULTS

Numerical study was conducted by using finite volume method ANSYS Fluent 12.1 with $k-\epsilon$ turbulence model as three dimensional steady state for experimental work carried out by placing binary building.

The finite volume method is based on the principle of dividing the geometry which will be solved in portions to find a solution for each of these sections and then by uniting these solutions to find a general solution to the problem. This method uses a technique which is based on the control volume for transforming heat flow equations into algebraic equations which can be solved numerically. In other words, this technique is based on the

principle of taking the heat flow equations integration in each control volume. This integration result provides equations which characterize each control volume which occurs. For preparing the most appropriate grid model, a fine grid should be formed in regions where the change in variables such as velocity, pressure and temperature is bigger. Therefore, the finest grid was used for the volume zones around the model building and in other zones a sparser grid was preferred. In the numerical model, the model with rooftop included 1381920 cells and without rooftop existed 74000 cells. Convergence of the computations was stopped for the continuity and the momentum equations when residues were less than 10^{-4} and for the energy equation when residues were less than

10^{-7} . A grid structure which consisted of pyramid shaped as three dimensional was used for simulation (Fig. 21).

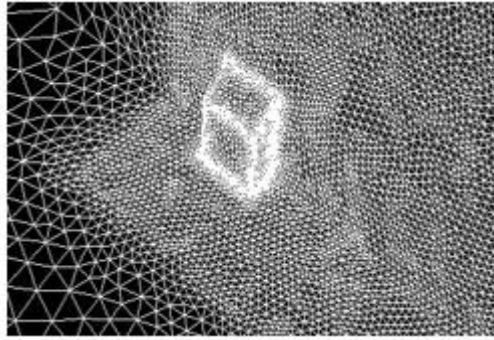


Figure 21. Mesh structure.

Because the buildings cause to turbulence in the flow, k-ε turbulence model which is frequently used in aerodynamic was employed as turbulence model in the numerical study, whereas the flow field was assumed to be laminar for channel.

The flow and heat transfer through the geometry are governed by the partial differential equation derived from the laws of conservation of mass, momentum and energy with steady state conditions without a body force, which are expressed as follows [7, 9,12].

Continuity equation

$$\frac{\partial u}{\partial x} + \frac{\partial v}{\partial y} + \frac{\partial w}{\partial z} = 0 \quad (1)$$

Momentum equation

x momentum equation

$$\rho \left(u \frac{\partial u}{\partial x} + v \frac{\partial u}{\partial y} + w \frac{\partial u}{\partial z} \right) = -\frac{\partial p}{\partial x} + \mu \left(\frac{\partial^2 u}{\partial x^2} + \frac{\partial^2 u}{\partial y^2} + \frac{\partial^2 u}{\partial z^2} \right) \quad (2.1)$$

y momentum equation

$$\rho \left(u \frac{\partial v}{\partial x} + v \frac{\partial v}{\partial y} + w \frac{\partial v}{\partial z} \right) = -\frac{\partial p}{\partial y} + \mu \left(\frac{\partial^2 v}{\partial x^2} + \frac{\partial^2 v}{\partial y^2} + \frac{\partial^2 v}{\partial z^2} \right) \quad (2.2)$$

z momentum equation

$$\rho \left(u \frac{\partial w}{\partial x} + v \frac{\partial w}{\partial y} + w \frac{\partial w}{\partial z} \right) = -\frac{\partial p}{\partial z} + \mu \left(\frac{\partial^2 w}{\partial x^2} + \frac{\partial^2 w}{\partial y^2} + \frac{\partial^2 w}{\partial z^2} \right) \quad (2.3)$$

In the equations, ρ is density, μ dynamic viscosity, p pressure, k thermal conductivity, T temperature, c_p specific heat and u,v,w are velocities of the x, y and z direction, respectively.

In the used standard k-ε turbulence model, the turbulence kinetic energy k' and its rate of dissipation ε, and the viscous dissipation term φ are used.

Steady flow turbulence kinetic energy equation

$$\frac{\partial(\rho uk')}{\partial x} + \frac{\partial(\rho vk')}{\partial y} + \frac{\partial(\rho wk')}{\partial z} = \frac{\partial}{\partial x} \left(\frac{\mu_t}{\sigma_k} \frac{\partial k'}{\partial x} \right) + \frac{\partial}{\partial y} \left(\frac{\mu_t}{\sigma_k} \frac{\partial k'}{\partial y} \right) + \frac{\partial}{\partial z} \left(\frac{\mu_t}{\sigma_k} \frac{\partial k'}{\partial z} \right) + \mu_t \phi - \rho \varepsilon \quad (3)$$

Turbulent viscosity

$$\mu_t = C_\mu \cdot \rho \cdot \frac{k'^2}{\varepsilon} \quad (4)$$

Turbulence kinetic energy

$$k' = \frac{1}{2} (\overline{u^2} + \overline{v^2} + \overline{w^2}) \quad (5)$$

Viscous dissipation term

$$\phi = 2\mu \left[\left(\frac{\partial u}{\partial x} \right)^2 + \left(\frac{\partial v}{\partial y} \right)^2 \right] + \mu \left(\frac{\partial v}{\partial x} + \frac{\partial u}{\partial y} \right)^2 \quad (6)$$

Turbulence kinetic energy disappearance equation

$$\frac{\partial(\rho u \varepsilon)}{\partial x} + \frac{\partial(\rho v \varepsilon)}{\partial y} + \frac{\partial(\rho w \varepsilon)}{\partial z} = \frac{\partial}{\partial x} \left(\frac{\mu_t}{\sigma_\varepsilon} \frac{\partial \varepsilon}{\partial x} \right) + \frac{\partial}{\partial y} \left(\frac{\mu_t}{\sigma_\varepsilon} \frac{\partial \varepsilon}{\partial y} \right) + \frac{\partial}{\partial z} \left(\frac{\mu_t}{\sigma_\varepsilon} \frac{\partial \varepsilon}{\partial z} \right) + C_{1\varepsilon} \mu_t \frac{\varepsilon}{k'} \phi - C_{2\varepsilon} \rho \frac{\varepsilon^2}{k'} \quad (7)$$

The model constants C_μ , $C_{1\varepsilon}$, $C_{2\varepsilon}$, σ_k and σ_ε have typically default values for used standard k- ε turbulence model [7, 9,12]. The values of these constants have been arrived at by numerous iterations of data fitting for a wide range of turbulent flows. These are as follows; $C_\mu=0.09$, $C_{1\varepsilon}= 1.44$, $C_{2\varepsilon}= 1.92$, $\sigma_k= 1$ and $\sigma_\varepsilon= 1.3$.

However, numerical model was carried out by using experimental environment conditions. Therefore, the numerical study was implemented for flow structure around the building models in the case of $z/H=0.5$ at x-z planes. Three dimensional detailed flow structures around the binary models were obtained for the case of 0.193 m/s flow velocity. Because the average turbulence intensity was fairly low (0.5%) at the inlet of the water channel, uniform velocity profile, u_∞ was applied in the numerical work at the channel inlet. Symetry and wall boundary conditions were used near the ceiling surface areas and model surfaces and plate, respectively. Outflow boundary condition was performed for the channel flow.

In Fig. 22, it was aimed to examine the flow structures occurred in front, side and back areas of the buildings and interactions with one another according to distances of the buildings to each other for models A placed as binary. Therefore, the variation of the time averaged u velocity component according to channel height were researched experimentally and numerically for certain areas of the building as dimensionless. When the graphs were investigated, it was seen that there was 2% difference between the experimental and numerical results for some areas. These differences were especially obtained at the rooftop sections of the building. However, the difference was very little at the front and back sides of the building. It is considered that the reason of this difference is due to continuous variability of the flow at the especially top sections of the building and not forming of the numerical and experimental conditions at the exactly same conditions. The building side and back areas give an idea about vortex formation. Besides, buildings seen in the graph were drawn without scale.

The flow structures were researched around the binary building models of B in Fig. 23. 2% difference was obtained between the numerical and experimental results. According to acquired

results, this difference occurred at the back sides of the building and it was very little at the front section of the building.

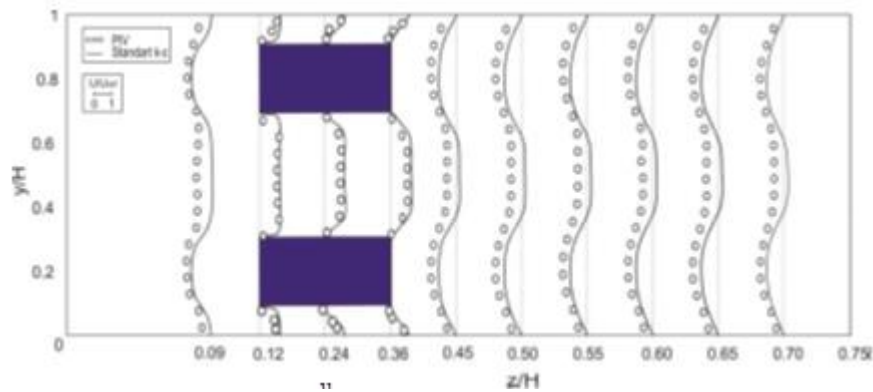


Figure 22. Velocity profiles ($\frac{u}{u_\infty}$) at $z/H=0.5$ symmetry surface for binary models of A.

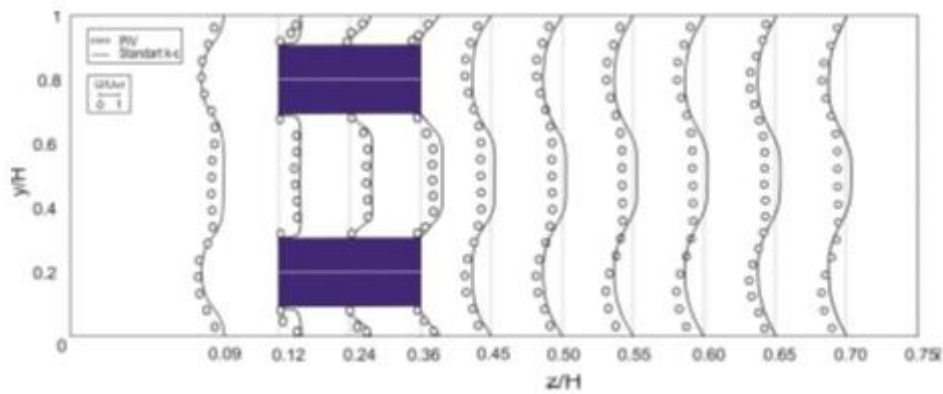


Figure 23. Velocity profiles ($\frac{u}{u_\infty}$) at $z/H=0.5$ symmetry surface for binary models of B.

In Fig. 24, the flow structures around the building models which one of them is without rooftop (model A) and another is with roof and 30° inclined (model B) were investigated. As it was seen that

there was a difference of 3% at some regions when Fig. 24 was researched, this difference increased at front and rear of the building.

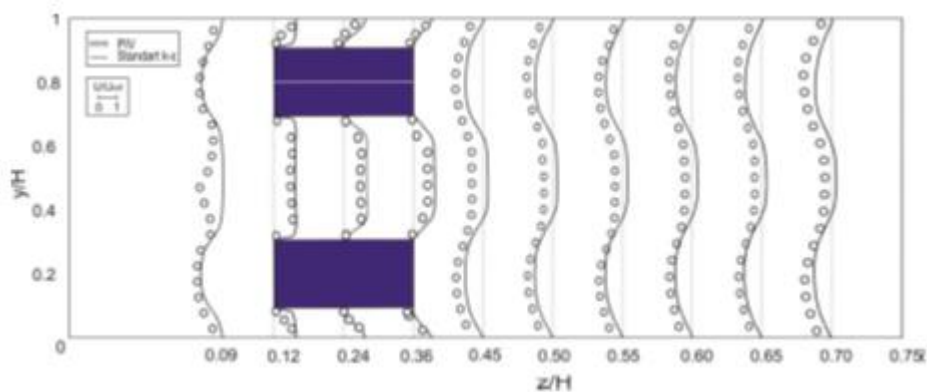


Figure 24. Velocity profiles ($\frac{u}{u_\infty}$) at $z/H=0.5$ symmetry surface for binary models of A and B.

7. RESULTS AND EVALUATION

The separation zones resulting from the wind interaction between the building and its immediate surroundings are of great importance for determining the wind forces acting on the buildings, multiple vortex systems interacting with the building and for considering the appropriate design parameters. The flow structure on the building is the first degree factor in dispersing of air pollutants into and around of the building. In order to find of these effects, air movements outside the building should be determined. The flow vortex movements seen in front of the building cause by raising particles such as dust, soil, leaves, rain and snow found in ground level. For these reasons, the knowledge of the flow structure and physic on the building contributes in terms of solving both design and technical problems.

In this study, flow structures around building models without rooftop at dimensions of 5x5x5cm and at dimensions of 5x5x5cm with 30° inclined and rooftop were investigated firstly by placing buildings by one by and afterwards they were analysed by leaving a distance of 13.75cm as binary placed (without rooftop, with rooftop and with and without rooftop) and using Particle Image Velocimetry (PIV) in water channel with closed circuit and open surface. The flow areas on these building models were examined and the following results was reached:

1. As a result of the separating of coming wind from the side and corners of the buildings, reverse flow regions occur in front, along the side walls, on the rooftop surface and behind of the buildings. Turbulance intensities increase in the mixture layer separating between reverse flow and free flow regions.

2. The vortex sizes in the rear of the building vary depending on the building geometries. It was composed the larger vortex regions in the building model with rooftop as it is moved away from the

model wall due to need for development distance of vortex regions and boundary layer development.

3. The flow velocities especially increase in the regions close to buildings depending on the distance between buildings due to jet flow between binary buildings. The trace regions formed in rears of building and the development distance changed. It was seen distinct increases in the lengths of the vortexes formed rear of the building models with rooftop.

4. When the experimental and numerical results were compared, it was seen that the flow profiles generally conformed with each other and the differences were in the regions behind the building.

8. NOMENCLATURE

| | |
|------------|--|
| ψ | Stream line |
| V | Vector region |
| ω | Vortex (peer level) |
| H | Building height (cm) |
| X | Vortex length (cm) |
| Na | Flow separation |
| Sa | Building front stop point |
| SI | Stop point (Saddle point) |
| F | Vortex |
| k | Thermal conductivity, (W/m.K) |
| k' | Turbulance kinetic energy, (m^2/s^2) |
| u, v, w | Velocity components of x,y,z directions, (m/s) |
| u',v',w' | Fluctuating velocity components in x,y,z directions, (m/s) |
| x, y, z | Cartesian coordinates, (m) |

Greek Symbols

| | |
|---------------|---|
| ε | Turbulent dissipation rate, (m^2/s^3) |
| μ | Dynamic viscosity, (kg/s.m) |
| μ_t | Turbulent viscosity, (kg/s. m) |
| ρ | Density, (kg./m ³) |
| ϕ | Viscous dissipation term, (m^2/s^3) |
| ν | Kinematic viscosity, (m^2/s) |

Acknowledgement

The authors would like to thank Scientific Research Projects Coordination Unit of Cumhuriyet University (Sivas/Turkey) for their financial support to this research under project number M-531.

REFERENCES

- [1] Park C.W. and Lee S.J., Effects of Free End Corner Shape on Flow Structure Around A Finite Cylinder, *J. Fluids Struc.*, 19-2 (2004) 141-158.
- [2] Zdravkovich M.M., Brand V.P., Maathew G., Weston A., Flow Past Short Circular Cylinders with Two Free Ends, *J. Fluid Mech.*, 203 (1989) 557-575.
- [3] Tutar M. and Oguz G., Large Eddy Simulation of Wind Flow Around Paralel Buildings with Varying Configurations, *Fluid Dynamics Research*, 31-5 (2002) 289-315.
- [4] Blocken B. and Carmeliet J., The Mutual Influence of Two Buildings on Their Wind Driven Rain Exposure and Comments on the Obstruction Factor, *J. Wind Eng. Ind. Aerodyn.*, 97-5 (2009) 180-196.
- [5] Gölbaşı D., Buyruk E., Sahin B., Karabulut K., Experimental and Numerical Investigation of Fluid Areas for Different Buildings Models, *MMO Tesisat Mühendisliği Dergisi*, 162 (2017) 32-47.
- [6] Gölbaşı D., Buyruk E., Sahin B., Karabulut K., Kılinc F., Experimental and Numerical Investigation of the Effect of Building Height Variation on the Flow Structures, 21. Ulusal Isı Bilimi ve Tekniği Kongresi, 356-366, 13-16 September 2017, Çorum.
- [7] Blocken B. and Stathopoulos T., CFD Simulation of Near Field Pollutant Dispersion on A High Resolution Grid: A Case Study by Les and Rans for A Building Group in Downtown Montreal, *Atmospheric Environment*, 45 (2011) 428-438.
- [8] Yan B.W. and Li Q.S., Wind Tunnel Study of Interference Effects Between Twin Super-Tall Buildings with Aerodynamic Modifications, *J. Wind Eng. Ind. Aerodyn.*, 156 (2016) 129-145.
- [9] Temel U.N., Yan Yana Taşıt Geçişi Durumlarındaki Etkileşimlerin Meydana Getirdiği Akış Yapılarının İncelenmesi, Cumhuriyet Üniversitesi, Fen Bilimleri Enstitüsü, Doktora Tezi, 2003, 236s.
- [10] Anonim, PIV Çalışma Prensipleri, Available at: <http://www.dantecdynamics.com>. Retrieved February 11, 2018.
- [11] Guilmineau E., Computational Study of Flow Around A Simplified Car Body, *J. Wind Eng. Ind. Aerodyn.*, 96-6 (2008) 1207-1217.
- [12] FLUENT User's Guide, Fluent Inc., Lebanon, (2003), NH.